Confinement Mechanisms for Epigenetic Modifications of Nucleosomes

Jan Fabio Nickels and Kim Sneppen*
Niels Bohr Institute, University of Copenhagen, Copenhagen 2100, Denmark

(Received 19 April 2023; accepted 11 August 2023; published 5 September 2023)

Nucleosomes and their modifications often facilitate gene regulation in eukaryotes. Certain genomic regions may obtain alternate epigenetic states through enzymatic reactions forming positive feedback between nucleosome states. This opens the possibility of a runaway process where the whole genome becomes uniformly modified. How a system of nucleosome states maintains confinement is an open question. Here we explore a family of stochastic dynamic models with combinations of read-write enzymes. We find that a larger number of intermediate nucleosome states increases the robustness of linear spreading in models with only local positive feedback reactions and the degree of bistability under conditions with at least one nonlocal feedback reaction. Further, supplementing the positive feedback with one negative feedback acting over long distances along the genome enables confinement of epigenetic, bistable regions. Our study emphasizes the importance of determining whether each particular read-write enzyme acts only locally or between distant nucleosomes.

DOI: 10.1103/PRXLife.1.013013

I. INTRODUCTION

Chromatic regions can exhibit epigenetic cell memory by adopting one of two stable states: transcriptionally silent heterochromatin and transcriptionally active euchromatin. Both alternatives can pass on to the next generation without changes in the underlying DNA sequence [1,2]. Modeling such epigenetic regions revealed essential properties for bistability and heritability like positive feedback of the modifying enzymes, nonlocal interactions, and (implicit) cooperativity [3]. The basic model structure has been successfully modified to answer different questions and to model nucleosome-mediated epigenetics in various organisms, like in, e.g., *Schizosaccharomyces pombe* [4–6], *Saccharomyces cerevisiae* [7], *Plasmodium falciparum* [8], *Drosophila* [9,10], *Arabidopsis thaliana* [11,12], and embryonic stem cells [13,14].

Often bistable regions are short and show abrupt boundaries in ChIP-seq profiles of associated histone modifications. Two examples of relatively small bistable regions are the two mating-type regions HML and HMR (around 3 kb) *in budding yeast* [15,16] and the FLC locus in *A. thaliana* (around six kB) [11].

Other small, putative bistable regions are heterochromatic islands in fission yeast. These facultative heterochromatic regions have a characteristic size of around 3 kb and are influenced by external factors like iron [17] or caffeine [18]. These factors have been shown to regulate the expression of the putative demethylase *Epe1* or *Mst2*.

Although relatively large regions like the mating-type region in *S. pombe* are very well characterized and have been modeled extensively [4–6], mathematical modeling of smaller regions has been scarce. In particular, determining how small regions can remain bistable and heritable despite high direct modifications and noise levels remains elusive.

In addition to more uniformly distributed blocklike ChIP-seq profiles, many genomic regions exhibit a bell-shaped pattern with a high central peak and increasingly lower modification levels at the periphery. The coexistence of these distinct profiles suggests different modes of heterochromatic spreading from the nucleation center, even though the same proteins are often found at these different types of loci. Moreover, previous models often assume the region of interest to be perfectly isolated from its surroundings.

Models where confinement of histone modifications arises spontaneously only consider two states where one of the states can spread from nucleation sites [19–22] and which are not able to produce bistable behavior. That is, they cannot hold the same region in a state with predominately active nucleosome states or predominantly silent nucleosome states for several generations. Rather, to achieve confinement, these models strongly depend on (1) the permanent nucleation of heterochromatic nucleosomes from nucleation sites; (2) the assumption that only heterochromatic nucleosomes can spread via a read-write mechanism while euchromatic or unmodified nucleosomes do not spread but can only be directly deposited by turnover, transcription and other processes; (3) the assumption of the complete absence of direct methylation outside nucleation sites; and (4) the ratio of heterochromatic spreading and turnover (direct deposition of euchromatic nucleosomes) needs to be below a threshold value.

Other approaches include feedback between modification dynamics and three-dimensional (3D) chromosome folding [23–26] or explore possible effects of read-write enzymes that may act persistently along the chromosome [27].

*sneppen@nbi.ku.dk

Noticeably, Refs. [22,25,26] also consider titration of limiting factors involved in read-write enzyme activity as a possible limitation for uncontrolled spreading in 3D chromosomes. Although such large-scale limitations indeed are realistic [28], they would be unable to explain confinement involving only a fraction of a chromosome.

Our Results section is subdivided into three major parts. In Sec. II A we analyze an established model [19,20] with linear (nearest-neighbor only) spreading of H3K9me from a central nucleation site. The possibility of long-range nucleation or long-range positive feedback explored in Refs. [21,22] is also investigated. In all cases, these models assume that the silencing mark only spread via a read-write mechanism and cannot be deposited directly outside nucleation sites. Here we relax this constraint and allow some direct methylation modifications also outside the nucleation region, a process also suggested by the two-state model in Ref. [29]. We demonstrate that noise in the form of direct H3K9me rates outside the nucleation site strongly decreases confinement. Moreover, we find that additional intermediate states increase robustness against such modifications. These investigations go beyond Ref. [29].

Section II B examines the role of intermediate states in another context—namely in model structures that are inherently bistable due to the presence of long-range interactions and cooperativity. We find that for the same parameter values, more intermediate states increase the two-state behavior—time spent in stably silent and stably active chromatin states as opposed to a mixture of silent and active states. That is, in analogy to higher Hill coefficients in epigenetic switches [30], more intermediate states increase the robustness of bistability in the presence of a given noise level. Overall, our analysis emphasizes that more intermediate states increase the resistance to noise and enables a more expansive repertoire of functionalities.

In Secs. II C–II E, we theoretically explore mechanisms that allow small chromosomal regions to be both bistable and confined. The proposed models are constrained by consistency with previous models and experiments of more extended parts of the genome [3–6]. Furthermore, a combination of positive and one global negative feedback from the heterochromatic state enable confinement of a silent or bistable state even without local barriers. This allows us to compare to recent experimental data [16] where a small heterochromatic region becomes first bistable and then completely euchromatic on successive weakening of surrounding nucleation sites of heterochromatic nucleosomes.

II. RESULTS

A. Linear-spreading models need multiple recruitment steps for intrinsic confinement

To examine the necessary conditions and properties of confining histone modifications after being established, we first looked at a well-established linear-spreading model of histone modifications [19,20] that enables intrinsic confinement. The model is supported by the experimental observation that H3K9me3 marks propagate gradually and symmetrically from a nucleation center at a synthetically modified *Oct4* locus of pluripotent cells and fibroblasts. Nucleation occurs via HP1α that is selectively recruited to the nucleation site on chemical induction and that associates with H3K9me-specific histone methyltransferases (HMTs) like SETDB1 and SUV39h1/2 [32–35]. These HMTs have read-write properties that enable them to bind to H3K9-methylated nucleosomes (the same modification that they catalyze) and to subsequently methylate nearby nucleosomes via allosteric activation of their enzymatic domain [36,37]. Starting from unmodified nucleosomes (H3K9un), this read-write mechanism creates positive feedback, resulting in a symmetric, linear propagation of H3K9me marks from the nucleation site.

The model has only two parameters, the feedback rate $k+$ and the demethylation-rate $k-$ (see Methods). For simplicity, the nucleation rate is set to be the same as the feedback ($k+$). The model is simulated for a total of 50 000 time steps on a one-dimensional lattice with 257 sites (representing nucleosomes) starting from only H3K9un nucleosomes to ensure that the system settles to a steady state. At each time step, the central nucleosome and each nucleosome adjacent to an already-methylated nucleosome are methylated with a probability of $k+$, and demethylation happens with a probability of $k-$ at every nucleosome in the system. The authors found that the simulations create bell-shaped steady-state profiles of H3K9me confined to a central region up to a ratio of $\frac{k+}{k-} = 1.5$ without requiring any explicit barriers or insulators. Confinement is a consequence of relatively weak positive feedback.

The above model assumes that H3K9 methylation can only occur directly via nucleation sites or by recruitment through neighboring nucleosomes. However, while loss of methyl-groups (H3K9me to H3K9un state transitions) can occur at each nucleosome, direct methyl-group additions (H3K9un to H3K9me) are assumed to be completely absent. As in Ref. [29] we find this assumption overly idealized since the direct collision of histones with HMTs and thus direct methylation at each nucleosome is likely to still occur in addition to feedback reactions, albeit possibly with a much lower probability. Thus we first explore what effect a low rate of direct methylation ($k+$ direct) would have on the confinement of H3K9me marks.

Figure 1 investigates steady-state profiles when direct methylation reactions are 50 times less likely than demethylation reactions [Fig. 1(b)]. The model has been simulated for different $\frac{k_+}{k_-}$ values to obtain different steady-state methylation profiles [Fig. 1(d)]. Figure 1(e) displays the basal height of these profiles far from the peak as a function of $\frac{k_+}{k_-}$. One sees that the confinement is entirely lost, even for relatively small values of $\frac{k_+}{k_-}$ (black line).

Subsequently, we wondered whether an additional intermediate state subject to feedback from H3K9me would rescue intrinsic confinement even with the additional $k+$ direct reaction. Including one additional recruitment step in the model [Fig. 1(b)] results in perfect spatial confinement for $\frac{k_+}{k_-}$ up until a value of $\approx$2.4 with a sharp transition at that value (blue line). We also examined the width of the profiles at half-maximal peak size and found that a broad bounded profile is possible with the three-state model but not with the two-state model (see Figs. 1(d) and S1 in the Supplemental Material [31]).

Additionally, two-state and three-state models with local positive feedback and the additional property of

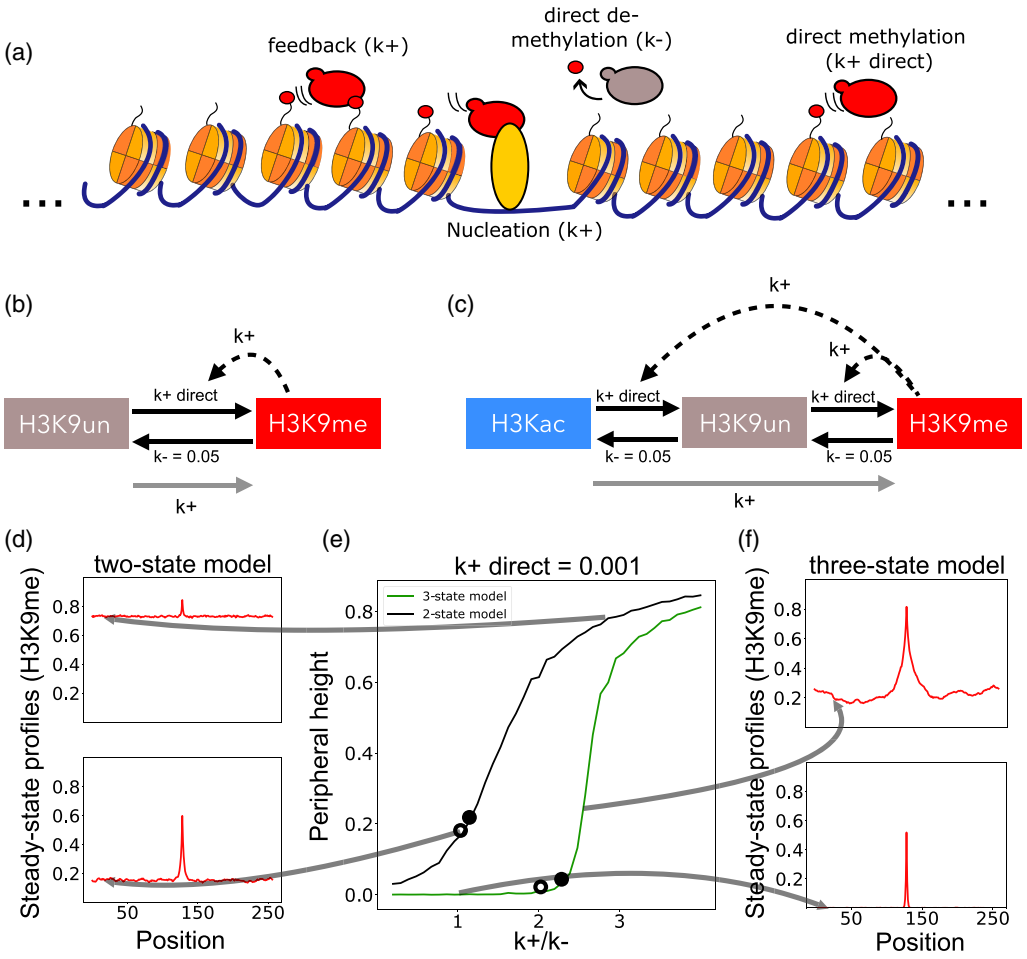

FIG. 1. An additional recruitment step from the H3K9me state increases the effectiveness of confinement in the presence of low direct silencing rates. (a) Illustration of all possible interactions of the basic linear spreading model. (b) Schematic of a two-state model with local positive feedback from H3K9me nucleosomes. (c) Schematic of a three-state model with local positive feedback from H3K9me nucleosomes. In both models, direct nucleosome conversions from methylated (H3K9me) to unmodified (H3K9un) are fixed at a rate of $k- = 0.05$ conversion attempts per nucleosome per time step and direct nucleosome conversions in the opposite direction (H3K9me to H3K9un) are fixed at a rate of 0.001 conversion attempts per nucleosome per time step. Gray arrows represent nucleation events, where only the central nucleosome is attempted to be converted. For simplicity, feedbacks (curved dashed arrows) and nucleation events are attempted with the same rate $k+$, whereas the value of $k+$ is varied in (e), resulting in a ratio $\frac{k+}{k-}$. [(d) and (f)] Example steady-state profiles showing the time-averaged enrichment of H3K9me-modified nucleosomes resulting from simulations corresponding to the $\frac{k+}{k-}$ values depicted by the curved arrows. (e) Relationship of the height at peripheral position 20 as a function of $\frac{k+}{k-}$ for the two-state and three-state models with fixed $k+ = 0.001$. Black open circles indicate conditions with a peak width of 10 nucleosomes at half-maximal peak height. Black full circles mark conditions with a width of 20 nucleosomes at half-peak height. See also Figs S1–S3 in the Supplemental Material [31].

long-range nucleation were tested. In these models, similarly to Refs. [21,22], nucleosomes are attempted to be converted at distance d with a probability of $\frac{1}{d}$ with distance d from the central recruiting region or nucleosome but positive feedback remains to occur only between nearest-neighboring nucleosome. In this case, additional recruitment steps also help confine methylated regions in the presence of small direct demethylation and acetylation rates (see Fig. S3 in the Supplemental Material [31]). Further, we tested a two-step model with long-range positive feedback (where nucleosomes interact with each other with probability $\frac{1}{d}$, where d is the distance between recruiting and substrate nucleosome) and local nucleation (Figs. S2(e) and S2(f) in the Supplemental Material [31]), confirming that this does not rescue confinement. This is in agreement with Ref. [20], where it was shown that positive feedback needs to occur primarily between nearest neighbors for inherent confinement, even in the overidealized case of no direct methylation outside nucleation sites.

In all cases we conclude that multistep recruitment reactions vastly increase the model's robustness against direct methylation of nucleosomes, effectively enabling the confinement of histone modifications surrounding a nucleation site.

So far, we only investigated spreading models, which cannot reproduce the fact that some chromosomal regions exhibit an all-or-none behavior, with rare but sudden transitions between alternative epigenetic states [1–3,5,11,16]. Robust bistability requires at least one nonlocal positive feedback [38] and is further strengthened by positive feedback in both

directions. Here nonlocal feedback is mediated by read-write enzymes that are able to bridge between nucleosomes that are distant along the DNA. A crucial unresolved question is how bistable chromosomal regions are intrinsically and robustly confined, which we will now explore by combining local and nonlocal reactions.

B. Multiple intermediate states increase robust epigenetics

Models often assume that nucleosomes can only adopt one of two or three states [19–21]. However, histone modifications often come in several degrees. For example, lysine 9 (H3K9me), lysine 36 (H3K36me), lysine 4 (H3K4me), and lysine 27 (H3K27me) often show multiple methyl groups. The read-write enzymes catalyzing the addition of these methyl groups bind their substrate and modify nearby or distant nucleosomes. PRC2, for example, binds to H3K27me3 histone tails via its RBBP4/7 subunit and catalyzes mono-, di-, and trimethylation of H3K27 on nearby nucleosomes (reviewed in Ref. [39]). This sequential addition of methyl groups may require subsequent independent binding and activity of the read-write enzyme, creating the possibility for nonprocessive multistep feedback. Indeed, Ref. [40] argues for such multistep recruitment of methylated marks in a model where the opposing reactions are mediated by transcription.

Here we explore how multiple recruitment steps influence the behavior of models that also allows for one or several nonlocal feedback reactions. The global feedback will allow every nucleosome to modify independently on relative positions while the local reactions are confined to nearest neighbors only. Our explorations presented here extend the previous analysis in Ref. [40].

We generically call the different nucleosome states A*, A, U, S, and S*, representing different modifications and modification degrees depending on the system in question. For example, one can think of the S and S* states as representing the PRC2-catalyzed H3K27me and H3K27me2/3 modifications and of the A* and A states as H3K4me and H3K4me2/3 modifications catalyzed by Trithorax [9]. Occasionally, we call the group of A* and A nucleosomes active due to their association with active gene expression states without making any claims about a causal connection with transcription itself. Conversely, we denote the combined group of S and S* states as silent nucleosomes due to their correspondence with silent gene expression states. The logic of several modification degrees can be extended to a seven-state model (see Fig. S4 in the Supplemental Material [31])

Due to the increased number of states and reactions of different types (local and global positive feedback conversions), the subsequent models are simulated by a Gillespie-type update.

Figure 2 explores different models with the same relative rate of spontaneous conversions and all implemented on a $L = 10$ system that is perfectly isolated from its surroundings. The type of positive feedback reactions is either global (occurring at long-range independent of position), shown with full arrows, or local (occurring only between neighbor nucleosomes), shown with dashed arrows. We performed the simulation at a relatively high fraction of spontaneous conversion attempts (30%) compared to actual positive feedback reaction attempts (see Methods for simulation details). The degree of bimodality is quantified through the normalized variance sampled over a very long simulation,

$$V_{\mathrm{norm}} = \frac{\mathrm{var(center)}}{\mathrm{len}^2}$$

where var is the variance of the state variables in a system with len = 10 the number of nucleosomes. The A state is assigned a value of −1, and the silenced state (S*) is assigned a value of +1. In Fig. 2, center = 10 is also the number of nucleosomes. The term "center" is used because later explorations consider the central subset of a larger system.

The normalized variance (V_{norm}) is shown in the upper left corner of each panel. The higher V_{norm}, the lower the switching rate between the two stable states. Here V_{norm} has a maximum of 100%, when the system spends an equal amount of time in the maximally silent (Silent-Active = 10) and the maximally active (Silent-Active = −10) and a minimum when the system spends all the time with a balanced mixture of states (Silent-Active = 0). In that random case the $V_{\mathrm{norm}} = 1/\mathrm{len} = 0.1$ as it reflects the variance of len = 10 independent numbers each with variance 1. Generally, all three-state models [Figs. 2(a), 2(c), and 2(e)] are marginally bimodal with a variance $V_{\mathrm{norm}} \sim 0.30$–$0.35$ of its maximal possible value, while the five-state models [Figs. 2(b), 2(d), and 2(f)] have a substantially higher variance of 0.57–0.75, marking robust bistability. One also notices weaker bistability for models with local feedback reactions that attack states more locally in the recruiting state space [Figs. 2(c) and 2(d)].

The results demonstrate that additional intermediate states increase the robustness of bistability, even if only a small subset of the feedback reactions are nonlocal Figs. 2(c)–2(f). Moreover, the probability distributions and variances of five-state and seven-state models are similar to three-state models with a squared or cubed spontaneous conversion parameter β (Fig. S4 in the Supplemental Material [31]).

The bimodality measure V_{norm} is similar to three-state models with a spontaneous conversion rate β^2 and a five-state model with β, while a three-state model with β^3 behaves as a seven-state model with β (see Fig. S4 in the Supplemental Material [31]). This is because each additional step between extreme states involves one more factor $\sqrt{\beta}$. This rescaling makes spontaneous transitions away from the minority state increasingly unlikely with a larger number of steps, which in turn causes the more stable bistability seen in Fig. 2 and Fig. S4 in the Supplemental Material [31]. An increase in overall robustness with an increased number of intermediate states was also explored in two-, three- and four-state models in Refs. [3,4,7]. The current investigation aims to systematize this, emphasizing that even adding more local feedback steps also substantially increases epigenetic memory. Altogether, we predict that small patches of nucleosomes may realistically exhibit bistable and epigenetic memory in themselves, provided that there are several intermediate states subject to nonlocal positive feedback. And this may be true even if only a small subset of the read-write recruitment reactions reaches beyond the nearest neighbor.

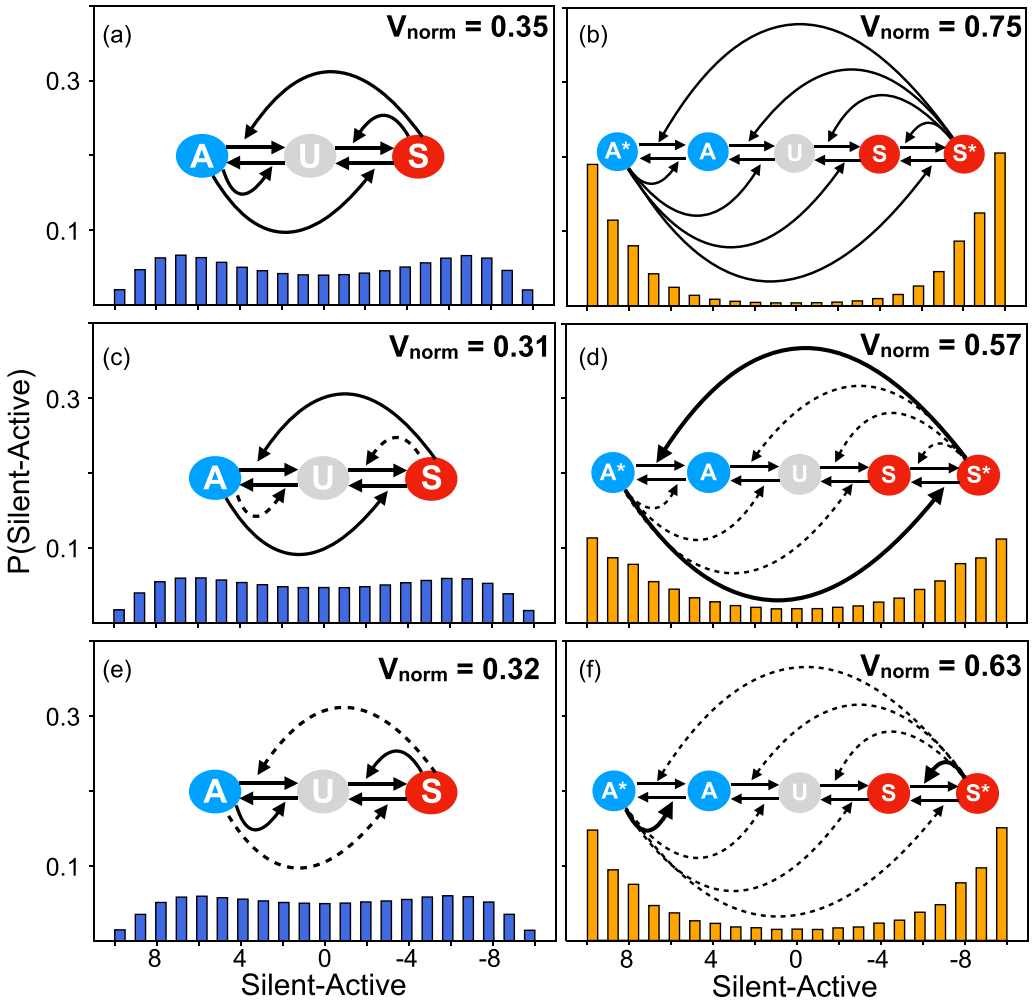

FIG. 2. Additional recruitment steps in models with nonlocal interactions and positive feedback from both sides (A/A* state and S/S* state) increases robust bistability. (a) The behavior of the classical three-state model with only global recruitment (solid arrow). At each update step, all recruitment types occur with equal probabilities of $\frac{1}{\text{total\_rate}}$ and all spontaneous conversion attempts occur with a probability of $\frac{0.3}{\text{total\_rate}}$ (30% of the rate of recruitment attempts) where total_rate $= \sum X_n$ and n is the number of reactions. [(c) and (e)] As in (a) but with a combination of local and nonlocal recruitment. Dashed lines denote reactions that only occur between neighbor nucleosomes. Three versions of three-state models (left panels) result in similar probability distributions with comparable variances (V_{norm}) in the number of silent-active nucleosomes. The analogous five-state models [(b), (d), and (f)] have a much higher value of V_{norm}, approaching the maximum bistability of $V_{\text{norm}} = 1$ for the $L = 10$ nucleosome system. See also Fig. S4 in the Supplemental Material [31].

C. Combined global negative and positive feedback enables localized epigenetics

Multiple positive feedback loops are necessary for the maintenance of alternative epigenetic states. However, what prevents a winning state from expanding across the entire genome has remained a puzzle. In the winner-takes-all dynamics the confinement of epigenetically stable states requires additional mechanisms that prevent unlimited spreading [7].

Naturally, confinement may be associated to heterochromatic boundaries. For example, in fission yeast, it has been shown that *Epe1*, a putative histone demethylase, is crucial for proper functioning of heterochromatic boundaries [17]. Interestingly, *Epe1* is recruited by *Swi6*, a reader of the heterochromatic state, and ChIP-seq profiles show that *Epe1* is enriched explicitly in heterochromatin. Moreover, Ref. [52] has shown that *Epe1* associates with the *SAGA-complex* that contains several histone acetylases (HATs).

Could models augmented with negative feedback from the silent nucleosome state enable the localization of bistable heterochromatic regions? To answer this question, we explored four-state models with one negative feedback reaction mediated by the S* state.

After examining models with distance-independent global feedback (see Figs. S6 and S7 in the Supplemental Material [31]) that enables localized bistability but were fragile and sensitive to system size, we used distance-dependent global feedback in simulations where nucleosomes interact with a probability that decreases as $\frac{1}{d}$ with increased distance d between nucleosomes. The observation that contact probabilities between nucleosomes decrease as a power law ($\frac{1}{d}$) with distance d between nucleosomes [55] justifies this choice. The model is based on many known interactions between modified nucleosomes and read-write enzymes [Fig. 3(a)] (see Fig. 5 in the Supplemental Material [31] for a description

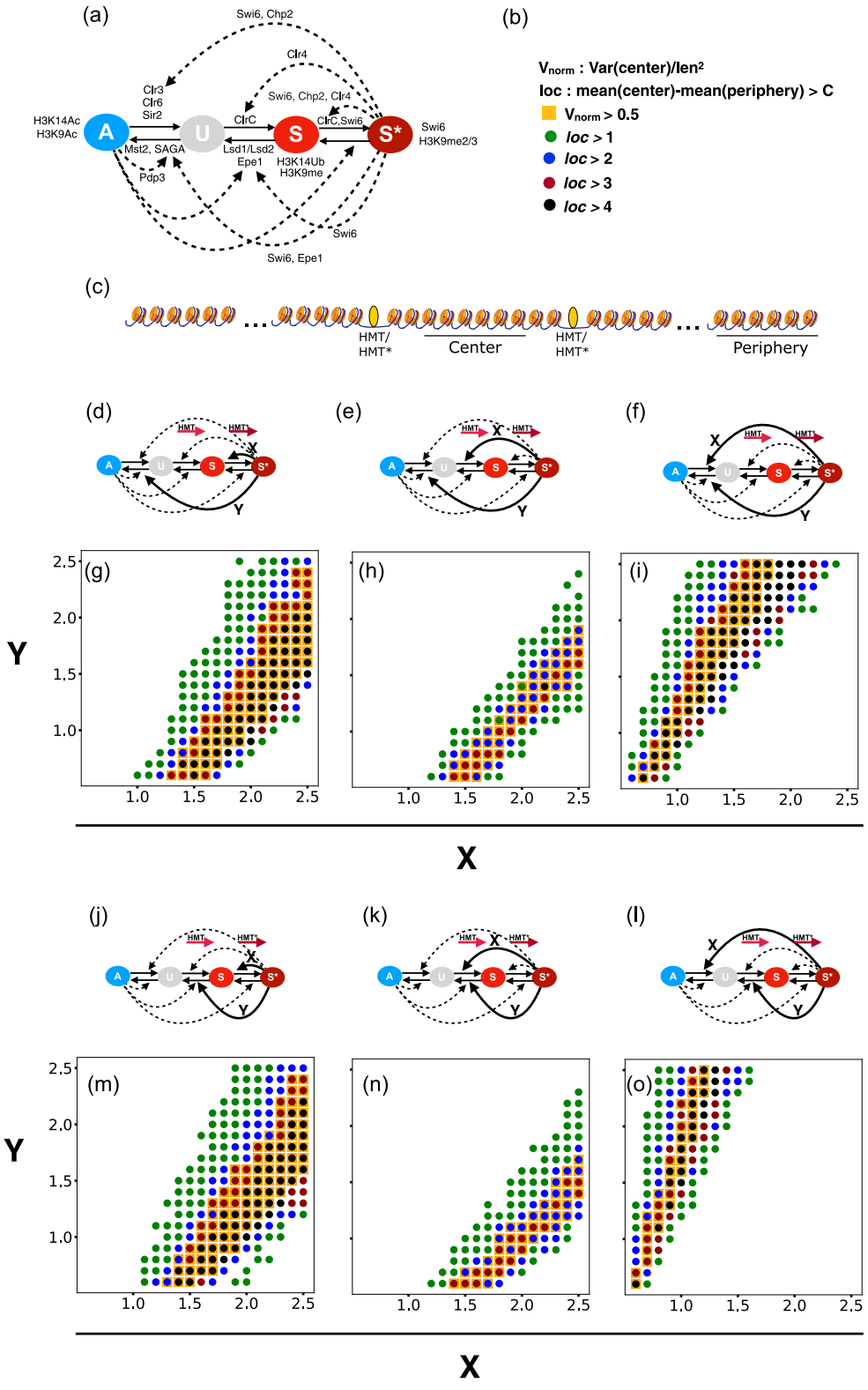

FIG. 3. Parameter scanning of models. (a) Four-state model structure based on known interactions between read-write enzymes and the modifications they read and write (see Fig. S5 in the Supplemental Material [31] for more details and Refs. [32,36,41–54]). (b) Bistability criterion and barrier measure. (c) Schematic of the system. Simulations considered a 40-nucleosome system without barriers and with two silencers. Figures 2(d)–2(f) and 2(j)–2(l) illustrate the used models. Straight, bold lines mark $1/d$ distance-dependent global feedback, while dashed lines mark local reactions. All local feedback rates are set to a value of 1 and all spontaneous conversion rates to a value of 0.05. The global feedback parameters X and Y were varied in scans (g)–(i) and (m)–(o). All models can exhibit localized bistability. Models (g) and (m) are the most robust as they predict most working parameters. See also the Supplemental Material [31] with Figures S6–S9. Figure S8 illustrates a case of confined bistability

and references). We posit that a subset of the enzymes could make use of the looping, while others might act only between neighboring nucleosomes.

The geometry of our model system is shown in Fig. 3(c), with a center region of 10 nucleosomes bounded by two silencers marked with yellow. These silencers are modeled as nucleosomes with a particularly high rate of spontaneous conversions to the S^* state. The region is embedded in a much larger system of in total 40 nucleosomes.

The degree of localization of the modification state is quantified by

$$\text{loc} = \text{mean(center)} - \text{mean(periphery)}.$$

Here the "center" is the difference between silent and active states for the six central nucleosomes located within the two nucleation sites. The "periphery" is the difference between silent and active states of the six rightmost nucleosomes in Fig. 3(c). The "mean" refers to a time average taken over a very long simulation.

The localization measure ranges between 0 (minimum) and 12 (maximum). However, since we are interested in localized bistability, a value of loc = 6 is already extremely high. Thus, the loc measure has values of 1, 2, 3, or 4 with larger loc indicating more effective confinement of the central region state from the outside regions. Additionally, we demanded that V_{norm} for the center be larger than 0.5 to count a parameter set as bistable [Fig. 3(b)]. This approximately corresponds to a distribution like the one seen in Fig. 2(d).

We did extensive parameter scanning of several model versions with one distance-dependent global negative and one distance-dependent global positive feedback, respectively. In each case, we tested for parameter values that provide confinement and bistability Figs. 3(d)–3(o). All tested models show regions of simultaneous confinement and bistability. However, the most robust models, in terms of the largest overlapping parameter space that enables localized bistability, were models with S*-mediated distance-dependent global S-to-S^* transitions [Fig. 3(d) and 3(j)].

Figure 4 shows simulation results of the same model as in Fig. 3(j) but with with a system size of $L = 80$ nucleosomes instead of $L = 40$ nucleosomes. This figure illustrates that the model with depicted parameter values [Fig. 4(b)] provides balanced prolonged active and silenced states between two silencers for several generations and stochastic switches between both metastable states. This results in a relatively high normalized variance V_{norm} of 0.68 and a mean around zero, as well as a low peripheral V_{norm} of 0.03 and a low mean of −5.5 [Fig. 4(b)]. Stochastic switches between stably active and silent states happen because the random appearance of A nucleosomes within the silencers may amplify themselves through local positive feedback, leading to a switch to an active region state that is only exposed to deacetylation from S^* nucleosomes on its periphery. On the other hand, when the region between the silencers is in the active state, randomly appearing S^* nucleosomes can result in switches from active to silent region states. Moreover, Figs S8 in the Supplemental Material [31] shows that this motif can sustain robust localized bistability despite regular disruptions caused by DNA replication.

Altogether, we find that four-state models with combined global negative and positive feedback enable localized bistable regions surrounded by euchromatin. Furthermore, this sharp separation between silenced and active regions of the genome did not need explicit barriers but instead required silencers in the form of strongly bound transcription factors.

In Ref. [40], transcription has been suggested to act as a global positive feedback from the active side. Thereby, the elongation of RNA polymerases on gene bodies may contribute to the confinement of some bistable regions. Our present analysis suggests another localization mechanism, using instead local positive feedback from active nucleosomes combined with longer-range negative feedback from silent states.

D. Global negative feedback and shape of noncentromeric H3K9me-profiles

Since many noncentromeric H3K9me3 domains in mammalian cells and heterochromatic islands in fission yeast have ChIP-seq profiles with localized peaks and soft borders [17], we asked whether our model can recapitulate these features. In Figs. 1 and Figs. S1–S3 in the Supplemental Material [31] we discuss the classical model for this phenomenon [19], pinpointing its weaknesses and a possible repair in terms of multistep recruitment processes. Here we suggest a scenario that is also robust to long-range positive feedback around the central inducing recruiting silencer and a relatively high degree of direct conversion attempts (5% of feedback attempts).

Figure 5 revisits the dynamics of the model from Fig. 4 and demonstrates that localized peaks of modifications can also be supported by increasing the strength of a long-range negative feedback. This allows for a localized methylation profile even in the presence of long-range positive feedback and high direct conversion rates (of 5% of recruitment rates). Figures 5(d)–5(f) illustrate that spatiotemporal fluctuations are large and persistent in time. Thus through the regulation of nucleosome modifications, we predict substantial cell-to-cell variations in gene expression [56] for promoters at moderate distance to such nucleation sites and levels of produced proteins [57]. We speculate that indirect gene regulation through epigenetic histone marks may provide yet another path to bursty gene regulation, beyond effects from persistent supercoiling variations [58,59] or strongly binding transcription factors [57,60].

E. Comparison with experimental data

Consistent with our analysis, Epe1 is recruited by Swi6 and is enriched at heterochromatic domains like the mating-type locus, peri-centromeres, and telomers, as well as heterochromatic islands [17,51]. More broadly, our model structure is consistent with known properties of read-write enzymes like positive feedback due to binding to nucleosomes modified with their substrate and subsequent allosteric activation of their catalytic activity leading to modifications of nearby nucleosomes (see Fig. S5 in the Supplemental Material [31]). Additionally, our modeling is consistent with the typical size of heterochromatic islands (around 3 kb) [51] and might

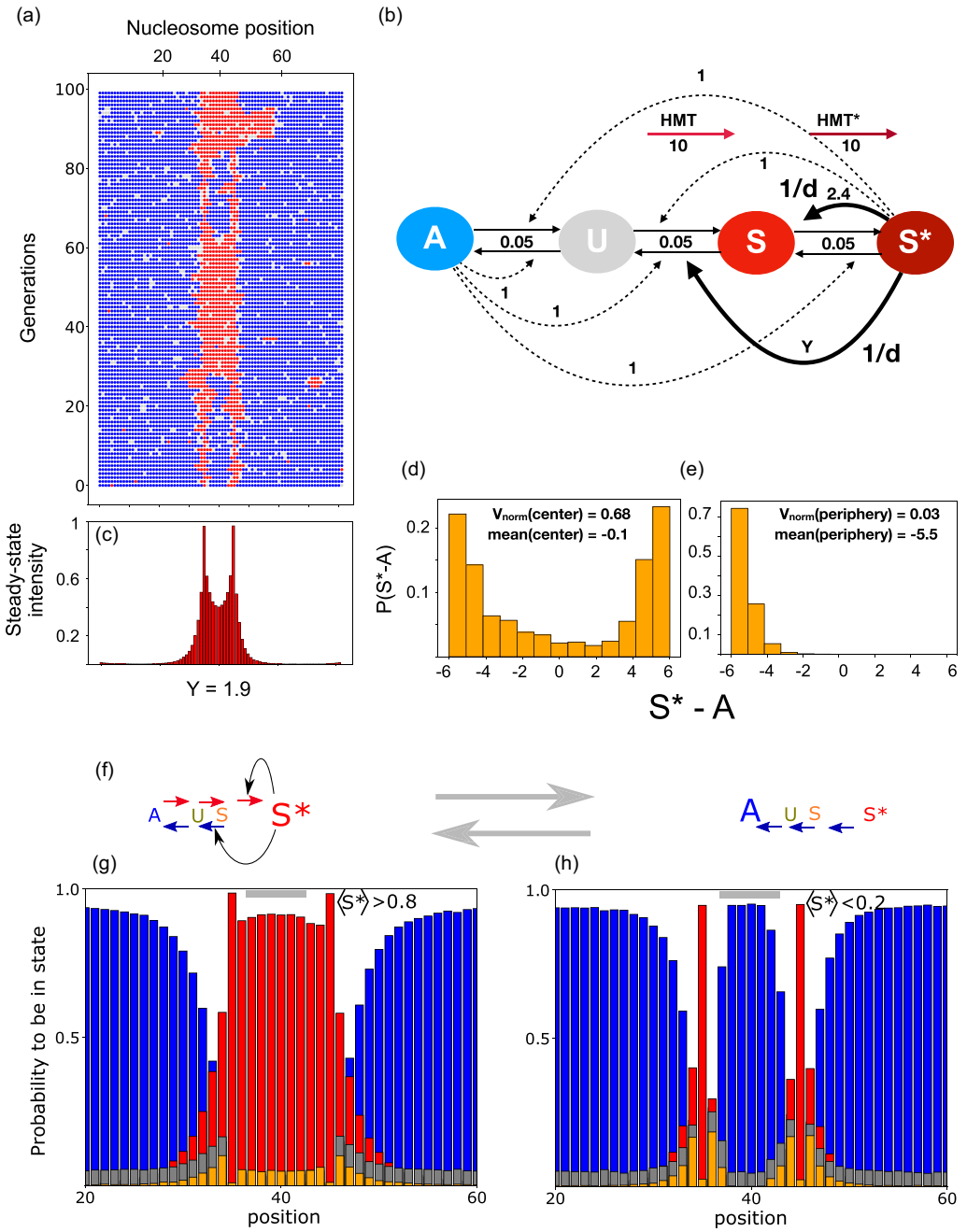

FIG. 4. Localization and bistability within two silencers using $1/d$ distance-dependent global negative and positive feedback shown in (b). (a) Example time-space plot of the model configurated as shown in (b) and corresponding steady-state enrichment profiles of S* nucleosomes (c). (d) Bi-modal distribution of nucleosome states within the two silencers. (e) Distribution of states outside the silencers. (f) The active global feedback and dominating local recruitment reactions (← or →) in silenced (left) respective active state (right). Panel (g) combined with (f) illustrates how S* changes StoU on just outside the silencers where U is present. This in turn allows further recruitment to an A state by a neighboring A (blue). As a result, the silenced region represses its own spreading. Panel (h) [with (f)] shows a dominating A state that maintains itself by local recruitments (blue ←). See also Fig. S10 in the Supplemental Material [31], which includes cell divisions.

explain why almost all of the *S. pombe* genome is enriched with acetylated histone modifications (euchromatin) [46,61].

Another experimental finding that agrees with our analysis is the ectopic spreading of heterochromatin in Epe1 deletion strains [70], as well as the expansion of heterochromatin at heterochromatic islands and the appearance of entirely new heterochromatic islands on Epe1 deletion [51].

An interesting observation of our modeling is that it can produce occasional ectopic spreading outside the confined region. This might explain the so-called position effect variegation, the spontaneous and stochastic silencing of genes incorporated into genomic loci close to heterochromatic regions [22,71,72].

Although bistable chromatin has been observed at the shortened mating-type region in *S. pombe* ΔK strains, direct

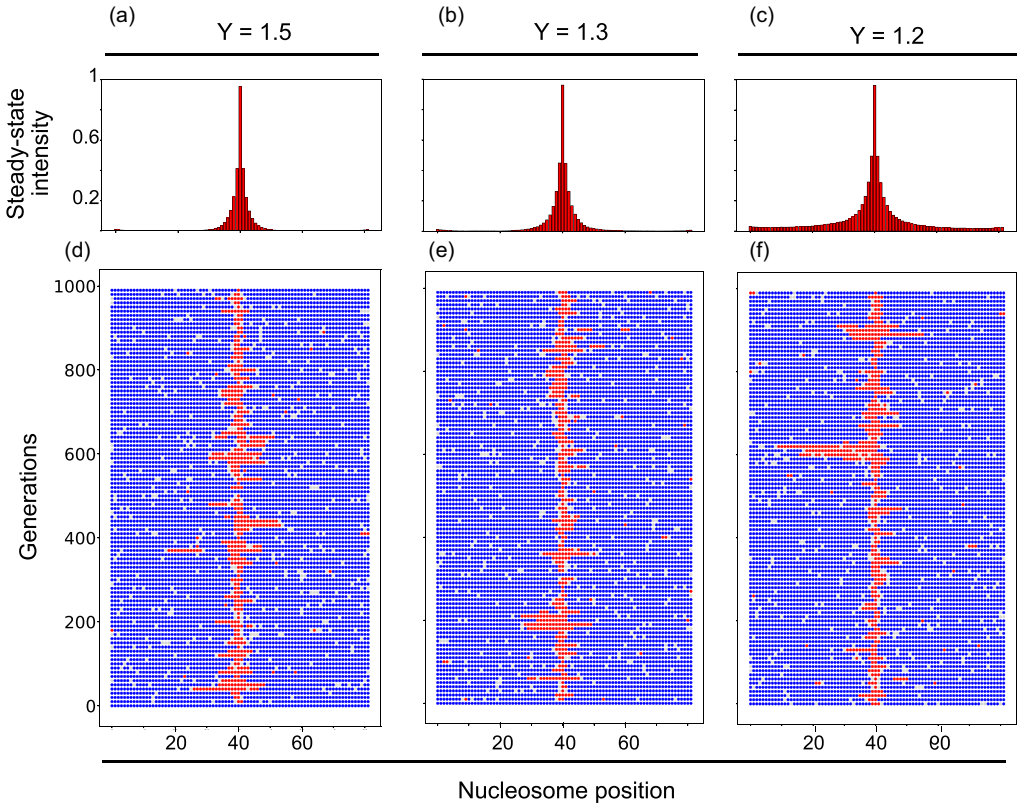

FIG. 5. Model from Fig. 4 but applied to a system with only one central nucleating site. One sees that such a system shows confinement when negative global feedback Y is large enough. This illustrates that observed nucleosome state profiles [19] can be obtained even in the presence of substantial nonrecruited conversions and long-range positive feedback. See also Fig. S11 in the Supplemental Material [31].

evidence for bistability of small regions in *S. pombe* is still missing. However, direct evidence for the bistability of small (2–4 kB) chromosomal regions exists in other organisms like budding yeast [16] or *A. thaliana* [11]. Our model predicts that suitable nucleation sites (around 10–15 nucleosomes) might generate bistable chromatic states in the encapsulated area when positioned close to each other. In the future, it will be interesting to test this hypothesis experimentally in *S. pombe* by, e.g., creating an artificial locus with nucleation sites like the *Atf1* binding site within the mating-type locus or different nucleation sites of heterochromatic islands.

Finally, epigenetic inheritance in bistable epigenetic regions often requires silencers or other protein-based memory elements [12,16,73] in addition to positive feedback. Interestingly, a recent study in budding yeast in Ref. [16] showed that the degree of bistability depends on both the degree of nucleation at silencers and positive feedback via recruited nucleosome conversions. In that study, the degree of nucleation at silencers has been modulated by deletions of several proteins that bind to the silencers E and I of the *HMRα* locus and which recruit the SIR complex [Fig. 6(b)]. The SIR complex consists of three subunits, SIR3, SIR4, and the histone-deacetylase SIR2. In budding yeast, the heterochromatic state (S^*) is characterized by a deacetylated and SIR-bound nucleosome state. Specifically, silencing occurs due to the recruitment of the SIR complex via nucleosomes that do not carry any active modifications (specifically H3K79me and H4K16ac) and subsequent deacetylation of nearby nucleosomes [74] (see Fig. S12(b) and S12(c) in the Supplemental Material [31]).

We tested our model against the findings of the above results [16]. To do this, we first identified parameters that predicted the whole region within both silencers to be almost entirely silenced while leaving the region outside the silencers active [Fig. 6(a)]. Subsequently, we weakened the nucleation strength (see Fig. 6 and Fig. S12 in the Supplemental Material [31]). In agreement with the experimental results in Ref. [16] [Fig. 6(d)], we found that the nucleation strength indeed determines the steady-state profiles of SIR4-bound nucleosome enrichment and the degree of bistability within the silencers (Fig. 6(c) and Fig. S12 in the Supplemental Material [31]).

Interestingly, mechanistic crosstalk between different types of active modifications and their read-write enzymes has been recently elucidated [68,69]. This crosstalk suggests multistep positive feedback processes from active and silent nucleosomes (see Fig. S12(b) in the Supplemental Material [31]). However, negative feedback remains to be shown in budding yeast. Our analysis suggests that one should search for additional read-write enzymes in this organism. Notice also that there are sharper boundaries between SIR4-enriched nucleosomes in experiments compared to simulations [Figs. 6(c) and 6(d)]. A simple extension of our model with an additional nucleation of active modifications close to the silencers but outside the *HMRα* region enables sharper boundaries in simulation due to synergy with the nucleation of silent nucleosomes at the silencers (see Fig. S12 in the Supplemental

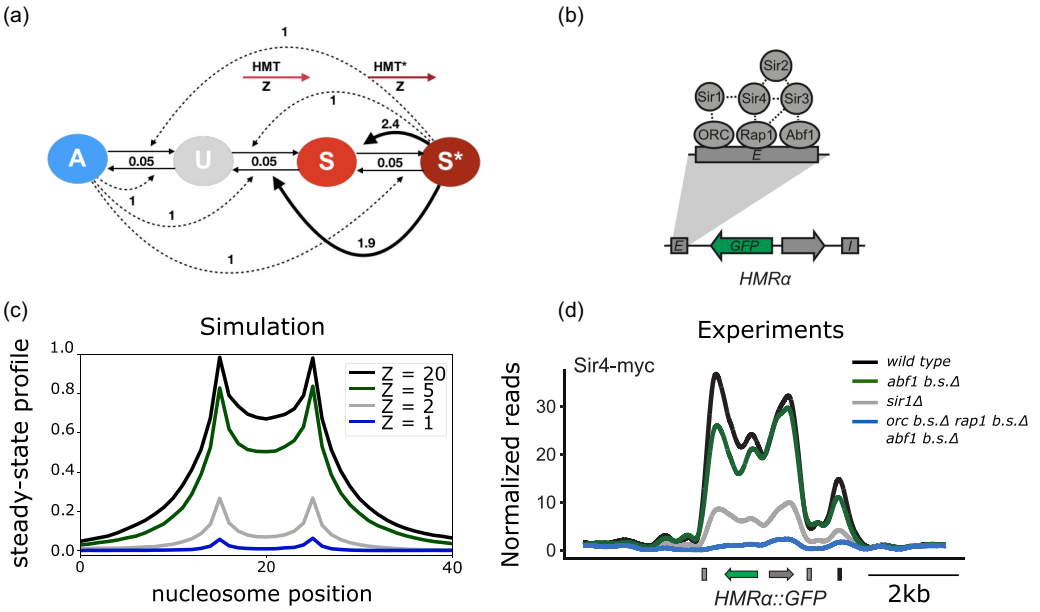

FIG. 6. Comparison of steady-state profiles and experimental ChIP-seq reads in *S. cerevisiae*. (a) Same model as in Figs. 4 and 5 but with fixed S*-mediated negative feedback and variable recruitment strength at the silencers (SIR $= Z$). Nucleation happens via local recruitment of the SIR complex to the silencers (see text and Fig. S12 in the Supplemental Material [31]). (b) Schematics adopted from Ref. [16] showing the different proteins involved in the recruitment of the SIR complex to the silencers. (c) Steady-state profile of time-averaged S*-nucleosome enrichment from simulations of the model and parameter values shown in (a) and with different degrees of direct SIR recruitment (SIR) at both silencers. Panel (d) is adapted from Ref. [16], showing ChIP-Seq profiles of Sir4-myc enrichment on the *HMRα::GFP* locus of different *S. cerevisiae* mutant strains where different combinations of boundary elements have been mutated. See Fig. S12 in the Supplemental Material [31] for more details and Refs. [16,62–69].

Material [31]). This is in line with the observation that active promoters close to the E and I silencers help prevent the ectopic spreading of Sir4 [75] to the surrounding euchromatic regions.

Overall, our theoretical analysis suggests that negative feedback could play a role in creating heterochromatic boundaries at the *HMRα* locus. It will be interesting to see whether such negative feedback exists as a part of a mechanism to prevent ectopic propagation of the SIR complex or whether boundaries in this organism rely on different mechanisms.

III. DISCUSSION

Localization phenomena are found across the natural sciences, from geology to physics and to life. In biology, it is associated with the specific control of or competition between the many diverse life processes. Within gene regulation, one may well argue that epigenetics in *trans* works so well by diffusive recruitment of regulators to promoters [76] that there is no need at all to bother about the more localized epigenetics in *cis* that may be provided through nucleosomes [77]. However, specificity and the ability to store the memory of cellular states locally on the genome will add another layer of regulation and increase the number of different states that a cell could take. For example, it allows the observed differentiation into hundreds of different olfactoric neuronal cells by using local positive feedback provided by nucleosomes read-write enzymes [78,79]. Furthermore, the spreading of histone marks from DNA-bound transcription factors may well facilitate the regulation of promoters, thus combining the best of the *cis* and the *trans* modes of regulation [38,80,81].

The current paper explored the ability to localize epigenetic marks around an inducing factor, for example, a silencer or a transcription factor. Across the genome, the main effect of nucleosome modifications is to maintain an externally regulated state in a 5- to 20-nucleosome region surrounding typical promoters. See Ref. [82] for a review that points out that histone modifications can be either a cause or consequence of genome function depending on the context. A simple setup of this type was provided by the one-step model [Fig. 1(a)] where one modification type is allowed to propagate between neighbors by locally acting read-write enzymes [19,20] (Figs. 1, S1, and S2) or via long-range positive feedback [21,22]. With the additional assumption of the complete absence of non-recruited conversions (like direct methylation), these models reproduce the observed localization of modifications with a spatial extension given by a ratio of spreading rate to decay rate for the modification in question. However, in a more realistic setting, each nucleosome is expected to be also modified by enzymes that are not associated with the particular region of interest or that directly bind and modify nucleosomes without being bound and activated by another nearby nucleosome. This direct methylation rate breaks the confinement and leads to varying degrees of unbounded escape from the region of interest (see Figs. 1 and Figs. S1 and S2(d) in the Supplemental Material [31]). One obtains a much more robust local spreading when one considers that nucleosomes in opposing epigenetic states are separated by more than one enzymatic reaction in the nucleosome state space. Just adding

one intermediate state, we find a finite threshold against direct conversions (see Figs. 1 and S1 and S2(g) and S2(h) in the Supplemental Material [31]). Figure 5 further demonstrates that possible negative feedback allows for localization even in the presence of long-range positive feedback. Noticeably, this mechanism works without limitations of enzymes relative to the substrate, which have been proposed as a possible confinement strategy on larger scales [7,22,25,26,83].

The remaining part of the paper focuses on metastable epigenetic states of systems of nucleosomes as seen in many real-world situations, from mating-type regions in yeast [1,2], over the memory of winter (vernalization) in plants [11] to the multiple states of olfactoric neurons in mammals [78]. We found that multistep separation of silenced and active nucleosome states with long-range positive feedback also opens for robust bistability [3], detailed further in Figs. 2–4. In this part of our analysis, the chromosomal region of concern is assumed to be perfectly isolated from its surroundings. We next asked how the winning epigenetic state is prevented from spreading across the chromosome. Such localization is difficult to obtain with only positive feedback, as it typically favors a runaway effect along the genome. This runaway effect is especially the case if we accept that some of the recruitment processes have to act nonlocally along the genome [3], and thereby bypass even quite broad barriers as explored in the 3D simulations in Ref. [24]. Perhaps more promising was the 3D simulation [23] where the spreading of locally dominating states was limited by externally imposed boundaries that favored the antagonistic state.

Combining positive and negative feedback is common in biology. In confinement and associated pattern formation, it has been suggested that Turing mechanisms play a role in the development of some organs [84,85]. Also, one has a Turing-like combination of local acting positive with more global negative feedback [78] acting through AdCy3 and LSD1 downregulation [79]. This mechanism allows the cell to select one and only one expressed olfactoric receptor protein.

Here we considered combined feedback of read-write enzymes between some fixed inducers or barriers on the chromosome. We found that such feedback could provide localized bistable regions, provided that the negative feedback was long range. Noticeably, there is a candidate for negative feedback using *Epe1* along the H3K9 modification axis in *S. pombe*. Currently, there is literature support for both indirect acetylase activity (as in Figs. 3(d)–3(f) and Figs. S6. (h) and S6(j), S7 and S8 in the Supplemental Material [31]) and a direct demethylase activity (as in Figs. 3(j)–3(l), Figs. 4–6 and Fig. S6(d) and S6(f) in the Supplemental Material [31]) Our analysis makes both scenarios workable.

A sampling of model variations suggests a need for long-range enzymatic conversions for both positive and negative feedback. In our sampling, we fixed parameters associated with direct conversions and local feedback reactions while varying the global feedback rates. These limitations on a more exhaustive parameter search were set by computational power, given the rather large number of reactions and unknown parameters. In agreement with [4–6] our exploration identified a persistent need for both global and local positive feedback. We here further found that localized bistability was easier to obtain when the global positive feedback reaction was acting closer to S^* than the global negative feedback reaction [Figs. 3(d) and 3(j)]. This translates into spatial recruitment reactions with negative feedback that acts at substantial distances from the silenced region [see Fig. 4(g)], thereby helping to maintain the active state in the surroundings.

Interestingly, recent evidence suggests that liquid-liquid droplet formation (phase separation) via $Swi6^{HP1}$ might contribute to the formation of heterochromatin under certain conditions [86,87]. This was modeled in the whole-chromosome-scale model in Ref. [26] assuming that HP1 was recruited by heterochromatin, which subsequently condensed to higher density with stronger HP1-mediated read-write activity between linearly distant nucleosomes [88]. Such separation might contribute to the confinement of heterochromatic regions, potentially in synergy with nonlocal negative feedback, as suggested in this paper. However, whether phase separation contributes to heterochromatin formation and/or maintenance is still controversial [89]. It is also unclear how the eventual droplets would maintain a specific size needed for confined but long-term heterochromatic silencing.

IV. CONCLUSION

Overall, our theoretical findings can be summarized as follows:

(i) Nonprocessive recruitment of read-write enzymes via eu- and heterochromatic nucleosomes and subsequent conversion of neighboring nucleosome states (multistep positive feedback) allows for increasingly robust confinement in linear spreading models.

(ii) Multistep positive feedback increases the bistability and robustness of models, even if only one positive feedback reaction occurs at long range.

(iii) Long-range negative feedback enables confinement in models with at least one long-range positive feedback reaction.

(iv) Distance dependence on nonlocal recruitment processes significantly increases the robustness of confinement.

(v) Multistep processes agree with observations of modification profiles and allow for controlled bistability through changed nucleation strength.

We particularly highlight the new suggestion that localized silencing or bistability could be obtained by supplementing positive feedback with a single negative feedback. Negative feedback with relatively strong activity directed from the inside to the outside of the silenced region. Candidates for such enzyme activities could be Epe1 or Mst2.

V. METHODS

A. Basic algorithm of purely local two-state models [Figs. 1(b), S1, and S2]

To ensure comparability with the model introduced in Ref. [19], we used a stochastic simulation algorithm (SSA) to simulate the models presented in Figs. 1, S1, and S2. We simulated the model on a one-dimensional lattice with 257 sites, each representing a nucleosome that can be in one of two states, H3K9un or H3K9me. Simulations were performed for 50,000 update steps, starting from all nucleosomes in

the H3K9un state, to ensure that the system has reached steady state.

The steady-state profiles show the time-averaged proportion of H3K9me nucleosomes at each lattice site. A nucleation reaction, a propagation reaction, a demethylation reaction (H3K9me to H3K9un) and a direct methylation reaction (H3K9un to H3K9me) is executed at each update step. Both nucleation and propagation reactions happen with a rate of $k+$. Demethylation reactions are fixed at a rate of $k- = 0.05$ and direct methylation reactions are fixed at $k + \text{direct} = 0.001$.

For the nucleation reaction, only the central nucleosome is attempted to be methylated, whereas the propagation reaction attempts to methylate every nucleosome that is the nearest neighbor of an already-methylated nucleosome at each update step. A turnover reaction (direct methylation or demethylation) consists of a specific direct conversion of each nucleosome in the system with the above-specified rate.

B. Basic algorithm of purely local three-state models [Figs. 1(c), S1, and S2]

The three-state model version [Fig. 1(c)] is simulated similarly to the two-state model but with an additional H3Kac state so that each nucleosome now exists in one of three states at each step. Simulations were performed for 100,000 update steps starting from all nucleosomes being in the H3Kac state. Also, there are now double as many different reactions. A nucleation reaction, two propagation reactions, and four direct modification attempts (acetylation (H3K9un to H3Kac) and a deacetylation reaction (H3Kac to H3K9un) in addition to the demethylation and direct methylation reaction of the two-state model) are executed at each update step. Both nucleation and propagation reactions happen with a rate of $k+$. A nucleation reaction consists of an attempt to directly convert the central nucleosome to the H3K9me state. For the feedback acting on H3K9un nucleosomes, all H3K9un nucleosomes that are the nearest neighbor of an H3K9me nucleosome are attempted to be converted to an H3K9me nucleosome. In the case of feedback acting on H3Kac nucleosomes, all H3Kac nucleosomes neighboring H3K9me nucleosomes are identified followed by a conversion attempt to an H3K9un nucleosome. Direct modifications are either fixed at a rate of $k- = 0.05$ if the direct transition is towards an active state (H3K9me to K3K9un or K3K9un to H3Kac) or at $k + \text{direct} = 0.001$ if the direct transition is towards a silent state (direct deacetylation or direct methylation). A turnover reaction consists of a specific direct conversion of each nucleosome in the system with the above-specified rate.

C. Basic algorithm

For all simulations that are not purely local as described above, the system is simulated as an agent-based model on a one-dimensional lattice with $N = 10$ sites (Fig. 2), $N = 40$ sites (Fig. 3), or $N = 80$ sites (Figs. 4–6), each representing a nucleosome that can be in one of several states. Nucleosome states are changed through different conversion types (events) that are selected based on an event-driven Gillespie algorithm. Subsequent decision on whether an event actually can occur between the chosen nucleosomes makes the simulation a hybrid algorithm where actual changes occur with rates that are smaller than the assigned rates in the Gillespie event selection.

Each event is one of n reaction types $1, 2, \ldots n$, and each event type is a spontaneous conversion, a recruited conversion, or a nucleation attempt. Reaction rates are defined as the average number of conversion attempts per nucleosome per time step. In Fig. S10 in the Supplemental Material [31], we simulated DNA replication by replacing each nucleosome in the system with U nucleosomes with 50% probability in regular intervals of 20 time steps. This introduces a timescale to our simulations. For example, in a cell that divides every 20 h, a time step would correspond to 1 h.

First, all rate constants are stored in a list ($\text{rates} = [X_1, X_2, \ldots, X_n]$), and a vector containing the cumulative sums of the rate constants ordered as in the rates list is created ($\text{cum}_{\text{rates}} = [X_1, X_1 + X_2, ..., X_1 + X_2 + \cdots + X_n]$). Then, for each update step, a random number (rand) uniformly distributed between 0 and the sum of all rate constants ($\text{total}_{\text{rate}} = \sum_{i=1}^{n} X_i$) is generated. The first index k where $\text{cum}_{\text{rates}}(k)$ is larger than $\text{rand} \cdot \text{total}_{\text{rate}}$ determines the event that is executed. The absolute time is increased by generating another random number (rand_1) and calculating $\tau = -\ln(\text{rand1})\frac{1}{\text{total\_rate}}$.

If a spontaneous conversion is attempted, then a random nucleosome in the system is chosen, and a state change is attempted accordingly (e.g., if a U-to-S conversion is attempted, a state change from U to S only happens if a U is selected).

In case of a recruited conversion, two nucleosomes (nuc1 = recruiting nucleosome and nuc2 = substrate nucleosome) are chosen and a state change happens if nuc1 and nuc2 are compatible with the chosen recruited reaction and then conversion is attempted. For example, if an S-nucleosome-mediated A-to-U transition [reaction S(A to U)] is chosen, then nuc2 changes its state from A to U if and only if only nuc1 is in the S state and nuc2 is in the A state).

Nucleation attempts are similar to spontaneous conversion, with the exception that a successful attempt requires the correct position in addition to the nucleosome being in the correct state (e.g., if the nucleation site is at position 40 and an UtoS nucleation is attempted, a state change from U to S only happens if nucleosome at position 40 is chosen and if it is in the U state).

It is important to note that rates are here defined as conversion attempts per nucleosome per time step, which is very different from successful conversions per time step that occur much more rarely and depend on the state of the system. For example, extensive model simulations (253 800 time steps), using the parameter values shown in Fig. 4, resulted in 2 413 353 successful feedback attempts of all possible feedback reactions (about 2.5 per generation). Similarly, there are 1 073 188 successful direct conversions of all potential direct conversion reactions (about 1 per generation per nucleosome). On average, each time step comprises approximately 9.5 successful feedback attempts and about 4.25 successful direct conversion attempts in the 80-nucleosome system. Consequently, the overall feedback-to-noise ratio is approximately 2.24, without considering nucleation attempts.

TABLE I. Reactions and reaction propensities with $A = \sum_{i=1}^{N} A_i$, $U = \sum_{i=1}^{N} U_i$, $S = \sum_{i=1}^{N} S_i$, and $A_i, U_i\, S_i \in \{0, 1\}$

Reaction key	Reaction	Reaction propensity
$\mathrm{A} \xrightarrow{\mathrm{HDAC}} \mathrm{U}$	$\mathrm{H3Kac} \xrightarrow{\mathrm{HDAC}} \mathrm{H3K9un}$	$c_1 A$
$\mathrm{U} \xrightarrow{\mathrm{HAT}} \mathrm{A}$	$\mathrm{H3K9un} \xrightarrow{\mathrm{HAT}} \mathrm{H3Kac}$	$c_2 U$
$\mathrm{U} \xrightarrow{\mathrm{HMT}} \mathrm{S}$	$\mathrm{H3K9un} \xrightarrow{\mathrm{HMT}} \mathrm{H3K9me}$	$c_3 U$
$\mathrm{S} \xrightarrow{\mathrm{HDM}} \mathrm{U}$	$\mathrm{H3K9me} \xrightarrow{\mathrm{HDM}} \mathrm{H3K9un}$	$c_4 S$
$\mathrm{A} \xrightarrow[\mathrm{S}]{\mathrm{HDAC}} \mathrm{U}$	$\mathrm{H3Kac} \xrightarrow[\mathrm{H3K9me}]{\mathrm{HDAC}} \mathrm{H3K9un}$	$c_5 SA$
$\mathrm{U} \xrightarrow[\mathrm{A}]{\mathrm{HAT}} \mathrm{A}$	$\mathrm{H3K9un} \xrightarrow[\mathrm{H3Kac}]{\mathrm{HAT}} \mathrm{H3Kac}$	$c_6 \sum_{i=1}^{N} A_i \frac{U_{i-1}+U_{i+1}}{2}$
$\mathrm{U} \xrightarrow[\mathrm{S}]{\mathrm{HMT}} \mathrm{S}$	$\mathrm{H3K9un} \xrightarrow[\mathrm{H3K9me}]{\mathrm{HMT}} \mathrm{H3K9me}$	$c_7 \sum_{i=1}^{N} S_i \frac{U_{i-1}+U_{i+1}}{2}$
$\mathrm{S} \xrightarrow[\mathrm{A}]{\mathrm{HDM}} \mathrm{U}$	$\mathrm{H3K9me} \xrightarrow[\mathrm{H3Kac}]{\mathrm{HDM}} \mathrm{H3K9un}$	$c_8 AS$

D. Local and global recruitment

In case the chosen event is local recruitment, nuc1 is chosen randomly and a neighboring nucleosome nuc2 is chosen as the left or right neighbor with equal probability. For a distance-independent global reaction, nuc1 and nuc2 are chosen randomly with nuc1 $\neq$ nuc2. A distance-dependent global reaction is executed by choosing nuc1 randomly and nuc2 at distance $d = |\mathrm{pos(nuc1)} - \mathrm{pos(nuc2)}|$ with probability $\frac{1}{d}$ (to the left or to the right of nuc1 with equal probability). A successful move requires nuc2 and nuc1 to be inside the region. When d is chosen, such that nuc2 is selected to be outside the region, nothing happens. To secure convergence, we select distance d within an interval that is at max the length of the simulated region.

E. Barriers

A barrier is implemented as a nucleosome in a permanent state (T state) that is not receptive to any involved modifications. An example could be that this position on the genome is bound by a specific transcription factorlike, e.g., CTCF.

F. Reaction propensities

Table I shows the reaction propensities of the model shown in Fig. 2(c) to illustrate the algorithm on an example.

G. Generations and DNA replication

We defined a generation to consist of 20 time steps as done in previous models [9]. The number of conversion attempts is on a similar scale as in Refs. [4,5] and our results are robust to an increase in cell generation but sensitive to the ratio of recruitment to direct conversions. We investigated the effect of DNA replication on localized bistability by simulating a state change of each nucleosome in the system to a U state with a 50% probability after each generation (see Fig. S10 in the Supplemental Material [31]).

H. Analysis

We generated the probability distributions in Fig. 2 and Fig. S3 in the Supplemental Material [31] from long simulations (10^9 update steps) starting from all nucleosomes in the U state. After each update step, the number of silent (S and S*) and active (A and A*) are counted and used for calculating the time-averaged probability distribution of silent-active nucleosomes.

Figure 4 and Fig. S7 in the Supplemental Material [31] show histograms of a bigger system subset of six respective nucleosomes. We simulated the system for 20 000 generations (about 10^9 update steps) and recorded the state of each nucleosome after each generation to generate these time-averaged distributions of states.

In the parameter-space plots (Fig. 3 and Figs. S6, S7, and S9 in the Supplemental Material [31]) two parameters are varied while fixing the remaining ones. For each parameter set, we run the simulations of 40 nucleosome systems for 10^8 update steps and test the system's properties. First, we highlight situations where the system exhibits bistability (orange); second, we grade the extent to which the system's interior differs from its exterior. Here the interior is defined within the silencing factors, while nucleosomes outside the barrier elements define the exterior.

Occasionally we illustrate the dynamics as space-time plots, displaying all nucleosomes in the system at several discrete time points. These plots allow us to present situations with qualitative differences between the dynamics in regions of the examined system. The time span we show is typically quite long, e.g., in Fig. 5 we show a time equivalent to 1000 generations.

ACKNOWLEDGMENTS

We thank the European Unions Horizon 2020 Research and Innovation Program under Marie Sklodowska Curie Grant No 813282 to J.F.N. for financial support. We also thank members of our group and especially our experimental collaborators, Genevieve Thon and her group members, for insightful discussions and guidance.

[1] S. I. Grewal and A. J. Klar, Chromosomal inheritance of epigenetic states in fission yeast during mitosis and meiosis, Cell **86**, 95 (1996).
[2] G. Thon and T. Friis, Epigenetic inheritance of transcriptional silencing and switching competence in fission yeast, Genetics **145**, 685 (1997).
[3] I. B. Dodd, M. A. Micheelsen, K. Sneppen, and G. Thon, Theoretical analysis of epigenetic cell memory by nucleosome modification, Cell **129**, 813 (2007).
[4] M. J. Obersriebnig, E. M. Pallesen, K. Sneppen, A. Trusina, and G. Thon, Nucleation and spreading of a heterochromatic domain in fission yeast, Nat. Commun. **7**, 11518 (2016).
[5] J. F. Nickels, A. K. Edwards, S. J. Charlton, A. M. Mortensen, S. C. L. Hougaard, A. Trusina, K. Sneppen, and G. Thon, Establishment of heterochromatin in domain-size-dependent bursts, Proc. Natl. Acad. Sci. USA **118**, e2022887118 (2021).
[6] J. F. Nickels, M. E. Della-Rosa, I. M. Goyeneche, S. J. Charlton, K. Sneppen, and G. Thon, The transcription factor atf1 lowers the transition barrier for nucleosome-mediated establishment of heterochromatin, Cell Rep. **39**, 110828 (2022).
[7] K. Sneppen and I. B. Dodd, Cooperative stabilization of the sir complex provides robust epigenetic memory in a model of sir silencing in saccharomyces cerevisiae, Epigenetics **10**, 293 (2015).
[8] V. M. Crowley, N. Rovira-Graells, L. R. de Pouplana, and A. Cortés, Heterochromatin formation in bistable chromatin domains controls the epigenetic repression of clonally variant plasmodium falciparum genes linked to erythrocyte invasion, Mol. Microbiol. **80**, 391 (2011).
[9] K. Sneppen and L. Ringrose, Theoretical analysis of polycomb-trithorax systems predicts that poised chromatin is bistable and not bivalent, Nat. Commun. **10**, 2133 (2019).
[10] J. Reinig, F. Ruge, M. Howard, and L. Ringrose, A theoretical model of polycomb/trithorax action unites stable epigenetic memory and dynamic regulation, Nat. Commun. **11**, 4782 (2020).
[11] A. Angel, J. Song, C. Dean, and M. Howard, A polycomb-based switch underlying quantitative epigenetic memory, Nature (London) **476**, 105 (2011).
[12] C. Lövkvist, P. Mikulski, S. Reeck, M. Hartley, C. Dean, and M. Howard, Hybrid protein assembly-histone modification mechanism for PRC2-based epigenetic switching and memory, eLife **10**, e66454 (2021).
[13] D. Holoch, M. Wassef, C. Lövkvist, D. Zielinski, S. Aflaki, B. Lombard, T. Héry, D. Loew, M. Howard, and R. Margueron, A cis-acting mechanism mediates transcriptional memory at polycomb target genes in mammals, Nat. Genet. **53**, 1686 (2021).
[14] K. Newar, A. Z. Abdulla, H. Salari, E. Fanchon, and D. Jost, Dynamical modeling of the H3K27 epigenetic landscape in mouse embryonic stem cells, PLoS Comput. Biol. **18**, e1010450 (2022).
[15] D. S. Saxton and J. Rine, Nucleosome positioning regulates the establishment, stability, and inheritance of heterochromatin in saccharomyces cerevisiae, Proc. Natl. Acad. Sci. USA **117**, 27493 (2020).
[16] D. S. Saxton and J. Rine, Distinct silencer states generate epigenetic states of heterochromatin, Mol. Cell **82**, 3566 (2022).
[17] M. Zofall, S. Yamanaka, F. E. Reyes-Turcu, K. Zhang, C. Rubin, and S. I. Grewal, Rna elimination machinery targeting meiotic mrnas promotes facultative heterochromatin formation, Science **335**, 96 (2012).
[18] S. Torres-Garcia, I. Yaseen, M. Shukla, P. N. Audergon, S. A. White, A. L. Pidoux, and R. C. Allshire, Epigenetic gene silencing by heterochromatin primes fungal resistance, Nature (London) **585**, 453 (2020).
[19] N. A. Hathaway, O. Bell, C. Hodges, E. L. Miller, D. S. Neel, and G. R. Crabtree, Dynamics and memory of heterochromatin in living cells, Cell **149**, 1447 (2012).
[20] C. Hodges and G. R. Crabtree, Dynamics of inherently bounded histone modification domains, Proc. Natl. Acad. Sci. USA **109**, 13296 (2012).
[21] F. Erdel and E. C. Greene, Generalized nucleation and looping model for epigenetic memory of histone modifications, Proc. Natl. Acad. Sci. USA **113**, E4180 (2016).
[22] A. Z. Abdulla, C. Vaillant, and D. Jost, Painters in chromatin: a unified quantitative framework to systematically characterize epigenome regulation and memory, Nucleic Acids Res. **50**, 9083 (2022).
[23] D. Michieletto, M. Chiang, D. Colì, A. Papantonis, E. Orlandini, P. R. Cook, and D. Marenduzzo, Shaping epigenetic memory via genomic bookmarking, Nucleic Acids Res. **46**, 83 (2018).
[24] D. Jost and C. Vaillant, Epigenomics in 3d: Importance of long-range spreading and specific interactions in epigenomic maintenance, Nucleic Acids Res. **46**, 2252 (2018).
[25] J. A. Owen, D. Osmanović, and L. A. Mirny, Design principles of 3d epigenetic memory systems, bioRxiv2022.09.24.509332 (2022).
[26] S. H. Sandholtz, Q. MacPherson, and A. J. Spakowitz, Physical modeling of the heritability and maintenance of epigenetic modifications, Proc. Natl. Acad. Sci. USA **117**, 20423 (2020).
[27] N. Ramakrishnan, S. R. B. Pillai, and R. Padinhateeri, High fidelity epigenetic inheritance: Information theoretic model predicts threshold filling of histone modifications post replication, PLoS Comput. Biol. **18**, e1009861 (2022).
[28] S. C. Elgin and G. Reuter, Position-effect variegation, heterochromatin formation, and gene silencing in drosophila, Cold Spring Harbor Perspect. Biol. **5**, a017780 (2013).
[29] M. Ancona, D. Michieletto, and D. Marenduzzo, Competition between local erasure and long-range spreading of a single biochemical mark leads to epigenetic bistability, Phys. Rev. E **101**, 042408 (2020).
[30] G. K. Ackers, A. D. Johnson, and M. A. Shea, Quantitative model for gene regulation by lambda phage repressor, Proc. Natl. Acad. Sci. USA **79**, 1129 (1982).
[31] See Supplemental Material at http://link.aps.org/supplemental/10.1103/PRXLife.1.013013 for brief description of additional model variants and literature support for the molecular interactions underlying the model structures. It also contains 12 supplementary figures labeled S1 to S12.
[32] S. Rea, F. Eisenhaber, D. O'Carroll, B. D. Strahl, Z. W. Sun, M. Schmid, S. Opravil, K. Mechtier, C. P. Ponting, C. D. Allis, and T. Jenuwein, Regulation of chromatin structure by site-specific histone H3 methyltransferases, Nature (London) **406**, 593 (2000).
[33] D. C. Schultz, K. Ayyanathan, D. Negorev, G. G. Maul, and F. J. Rauscher, SETDB1: A novel KAP-1-associated histone H3, lysine 9-specific methyltransferase that contributes to

HP1-mediated silencing of euchromatic genes by KRAB zinc-finger proteins, Genes Dev. **16**, 919 (2002).

[34] A. H. Peters, S. Kubicek, K. Mechtler, R. J. O'Sullivan, A. A. Derijck, L. Perez-Burgos, A. Kohlmaier, S. Opravil, M. Tachibana, Y. Shinkai, J. H. Martens, and T. Jenuwein, Partitioning and plasticity of repressive histone methylation states in mammalian chromatin, Mol. Cell **12**, 1577 (2003).

[35] L. Fritsch, P. Robin, J. R. Mathieu, M. Souidi, H. Hinaux, C. Rougeulle, A. Harel-Bellan, M. Ameyar-Zazoua, and S. Ait-Si-Ali, A subset of the histone H3 lysine 9 methyltransferases Suv39h1, G9a, GLP, and SETDB1 participate in a multimeric complex, Mol. Cell **37**, 46 (2010).

[36] K. Zhang, K. Mosch, W. Fischle, and S. I. Grewal, Roles of the Clr4 methyltransferase complex in nucleation, spreading and maintenance of heterochromatin, Nat. Struct. Mol. Biol. **15**, 381 (2008).

[37] B. Al-Sady, H. D. Madhani, and G. J. Narlikar, Division of labor between the chromodomains of HP1 and Suv39 methylase enables coordination of heterochromatin spread, Mol. Cell **51**, 80 (2013).

[38] K. Sneppen, M. A. Micheelsen, and I. B. Dodd, Ultrasensitive gene regulation by positive feedback loops in nucleosome modification, Mol. Syst. Biol. **4**, 182 (2008).

[39] P. Chammas, I. Mocavini, and L. D. Croce, Engaging chromatin: Prc2 structure meets function, Br. J. Cancer **122**, 315 (2019).

[40] S. Berry, C. Dean, and M. Howard, Slow chromatin dynamics allow polycomb target genes to filter fluctuations in transcription factor activity, Cell Syst. **4**, 445 (2017).

[41] S. Haldar, A. Saini, J. S. Nanda, S. Saini, and J. Singh, Role of Swi6/HP1 self-association-mediated recruitment of Clr4/Suv39 in establishment and maintenance of heterochromatin in fission yeast, J. Biol. Chem. **286**, 9308 (2011).

[42] M. R. Motamedi, E. J. E. Hong, X. Li, S. Gerber, C. Denison, S. Gygi, and D. Moazed, HP1 proteins form distinct complexes and mediate heterochromatic gene silencing by nonoverlapping mechanisms, Mol. Cell **32**, 778 (2008).

[43] T. Fischer, B. Cui, J. Dhakshnamoorthy, M. Zhou, C. Rubin, M. Zofall, T. D. Veenstra, and S. I. Grewal, Diverse roles of HP1 proteins in heterochromatin assembly and functions in fission yeast, Proc. Natl. Acad. Sci. USA **106**, 8998 (2009).

[44] T. Yamada, W. Fischle, T. Sugiyama, C. D. Allis, and S. I. Grewal, The nucleation and maintenance of heterochromatin by a histone deacetylase in fission yeast, Mol. Cell **20**, 173 (2005).

[45] P. Bjerling, R. A. Silverstein, G. Thon, A. Caudy, S. Grewal, and K. Ekwall, Functional divergence between histone deacetylases in fission yeast by distinct cellular localization and in vivo specificity, Mol. Cell. Biol. **22**, 2170 (2002).

[46] M. Wirén, R. A. Silverstein, I. Sinha, J. Walfridsson, H. M. Lee, P. Laurenson, L. Pillus, D. Robyr, M. Grunstein, and K. Ekwall, Genomewide analysis of nucleosome density histone acetylation and hdac function in fission yeast, EMBO J. **24**, 2906 (2005).

[47] N. Abshiru, R. E. Rajan, A. Verreault, and P. Thibault, Unraveling site-specific and combinatorial histone modifications using high-resolution mass spectrometry in histone deacetylase mutants of fission yeast, J. Proteome Res. **15**, 2132 (2016).

[48] J. Nakayama, J. C. Rice, B. D. Strahl, C. D. Allis, and S. I. Grewal, Role of histone H3 lysine 9 methylation in epigenetic control of heterochromatin assembly, Science **292**, 110 (2001).

[49] A. J. Bannister, P. Zegerman, J. F. Partridge, E. A. Miska, J. O. Thomas, R. C. Allshire, and T. Kouzarides, Selective recognition of methylated lysine 9 on histone H3 by the HP1 chromo domain, Nature (London) **410**, 120 (2001).

[50] K. I. Noma, T. Sugiyama, H. Cam, A. Verdel, M. Zofall, S. Jia, D. Moazed, and S. I. Grewal, Rits acts in cis to promote rna interference-mediated transcriptional and post-transcriptional silencing, Nat. Genet. **36**, 1174 (2004).

[51] M. Zofall and S. I. Grewal, Swi6/HP1 recruits a jmjc domain protein to facilitate transcription of heterochromatic repeats, Mol. Cell **22**, 681 (2006).

[52] K. Bao III, C. M. Shan, J. Moresco, J. Yates, and S. Jia, Anti-silencing factor Epe1 associates with SAGA to regulate transcription within heterochromatin, Genes Dev. **33**, 116 (2019).

[53] V. Flury, P. R. Georgescu, V. Iesmantavicius, Y. Shimada, T. Kuzdere, S. Braun, and M. Bühler, The histone acetyltransferase Mst2 protects active chromatin from epigenetic silencing by acetylating the ubiquitin ligase Brl1, Mol. Cell **67**, 294 (2017).

[54] F. Lan, M. Zaratiegui, J. Villén, M. W. Vaughn, A. Verdel, M. Huarte, Y. Shi, S. P. Gygi, D. Moazed, R. A. Martienssen, and Y. Shi, S. *pombe* LSD1 homologs regulate heterochromatin propagation and euchromatic gene transcription, Mol. Cell **26**, 89 (2007).

[55] T. Mizuguchi, G. Fudenberg, S. Mehta, J.-M. Belton, N. Taneja, H. D. Folco, P. Fitzgerald, J. Dekker, L. Mirny, J. Barrowman, and S. I. S. Grewal, Cohesin-dependent globules and heterochromatin shape 3D genomearchitecture in *S. pombe*, Nature (London) **516**, 432 (2014).

[56] S. J. Shareef, S. M. Bevill, A. T. Raman, M. J. Aryee, P. van Galen, V. Hovestadt, and B. E. Bernstein, Extended-representation bisulfite sequencing of gene regulatory elements in multiplexed samples and single cells, Nat. Biotechnol. **39**, 1086 (2021).

[57] A. Sanchez and I. Golding, Genetic determinants and cellular constraints in noisy gene expression, Science **342**, 1188 (2013).

[58] N. Mitarai, I. B. Dodd, M. T. Crooks, and K. Sneppen, The generation of promoter-mediated transcriptional noise in bacteria, PLoS Comput. Biol. **4**, e1000109 (2008).

[59] M. Ancona, A. Bentivoglio, C. A. Brackley, G. Gonnella, and D. Marenduzzo, Transcriptional bursts in a nonequilibrium model for gene regulation by supercoiling, Biophys. J. **117**, 369 (2019).

[60] N. Mitarai, S. Semsey, and K. Sneppen, Dynamic competition between transcription initiation and repression: Role of nonequilibrium steps in cell-to-cell heterogeneity, Phys. Rev. E **92**, 022710 (2015).

[61] I. Sinha, L. Buchanan, M. Rnnerblad, C. Bonilla, M. Durand-Dubief, A. Shevchenko, M. Grunstein, A. F. Stewart, and K. Ekwall, Genome-wide mapping of histone modifications and mass spectrometry reveal H4 acetylation bias and H3K36 methylation at gene promoters in fission yeast, Epigenomics **2**, 377 (2010).

[62] S. I. Imai, C. M. Armstrong, M. Kaeberlein, and L. Guarente, Transcriptional silencing and longevity protein Sir2 is an NAD-dependent histone deacetylase, Nature (London) **403**, 795 (2000).

[63] S. Ghidelli, D. Donze, N. Dhillon, and R. T. Kamakaka, Sir2p exists in two nucleosome-binding complexes

with distinct deacetylase activities, EMBO J. **20**, 4522 (2001).
[64] M. Brothers and J. Rine, Distinguishing between recruitment and spread of silent chromatin structures in saccharomyces cerevisiae, eLife **11**, e75653 (2022).
[65] R. G. Gardner, Z. W. Nelson, and D. E. Gottschling, Ubp10/dot4p regulates the persistence of ubiquitinated histone h2b: Distinct roles in telomeric silencing and general chromatin, Mol. Cell. Biol. **25**, 6123 (2005).
[66] J. A. Daniel, M. S. Torok, Z. W. Sun, D. Schieltz, C. D. Allis, J. R. Yates, and P. A. Grant, Deubiquitination of histone H2B by a yeast acetyltransferase complex regulates transcription, J. Biol. Chem. **279**, 1867 (2004).
[67] J. Y. Kang, J. Y. Kim, K. B. Kim, J. W. Park, H. Cho, J. Y. Hahm, Y. C. Chae, D. Kim, H. Kook, S. Rhee, N. C. Ha, and S. B. Seo, KDM2B is a histone H3K79 demethylase and induces transcriptional repression VIA sirtuin-1-mediated chromatin silencing, FASEB J. **32**, 5737 (2018).
[68] M. I. Valencia-Sánchez, P. D. Ioannes, M. Wang, D. M. Truong, R. Lee, J. P. Armache, J. D. Boeke, and K. J. Armache, Regulation of the Dot1 histone H3K79 methyltransferase by histone H4K16 acetylation, Science **371**, eabc6663 (2021).
[69] T. van Welsem, T. Korthout, R. Ekkebus, D. Morais, T. M. Molenaar, K. van Harten, D. W. Poramba-Liyanage, S. M. Sun, T. L. Lenstra, R. Srivas, T. Ideker, F. C. Holstege, H. van Attikum, F. E. Oualid, H. Ovaa, I. J. Stulemeijer, H. Vlaming, and F. van Leeuwen, Dot1 promotes H2B ubiquitination by a methyltransferase-independent mechanism, Nucleic Acids Res. **46**, 11251 (2018).
[70] M. Sorida, T. Hirauchi, H. Ishizaki, W. Kaito, A. Shimada, C. Mori, Y. Chikashige, Y. Hiraoka, Y. Suzuki, Y. Ohkawa, H. Kato, S. Takahata, and Y. Murakami, Regulation of ectopic heterochromatin-mediated epigenetic diversification by the jmjc family protein epe1, PLoS Genet. **15**, e1008129 (2019).
[71] R. C. Allshire, J. P. Javerzat, N. J. Redhead, and G. Cranston, Position effect variegation at fission yeast centromeres, Cell **76**, 157 (1994).
[72] M. B. Zerihun, C. Vaillant, and D. Jost, Effect of replication on epigenetic memory and consequences on gene transcription, Phys. Biol. **12**, 026007 (2015).
[73] D. S. Saxton and J. Rine, Epigenetic memory independent of symmetric histone inheritance, eLife **8**, e51421 (2019).
[74] R. Behrouzi, C. Lu, M. Currie, G. Jih, N. Iglesias, and D. Moazed, Heterochromatin assembly by interrupted sir3 bridges across neighboring nucleosomes, eLife **5**, e17556 (2016).
[75] D. Donze and R. T. Kamakaka, Rna polymerase iii and rna polymerase ii promoter complexes are heterochromatin barriers in saccharomyces cerevisiae, EMBO J. **20**, 520 (2001).
[76] M. Ptashne, Epigenetics: Core misconcept, Proc. Natl. Acad. Sci. USA **110**, 7101 (2013).
[77] B. M. Turner, Cellular memory and the histone code, Cell **111**, 285 (2002).
[78] A. K. Alsing and K. Sneppen, Differentiation of developing olfactory neurons analysed in terms of coupled epigenetic landscapes, Nucleic Acids Res. **41**, 4755 (2013).
[79] D. B. Lyons, W. E. Allen, T. Goh, L. Tsai, G. Barnea, and S. Lomvardas, An epigenetic trap stabilizes singular olfactory receptor expression, Cell **154**, 325 (2013).
[80] P. Korber and S. Barbaric, The yeast pho5 promoter: from single locus to systems biology of a paradigm for gene regulation through chromatin, Nucleic Acids Res. **42**, 10888 (2014).
[81] L. Ringrose and M. Howard, Dissecting chromatin-mediated gene regulation and epigenetic memory through mathematical modelling, Curr. Opin. Syst. Biol. **3**, 7 (2017).
[82] G. Millán-Zambrano, A. Burton, A. J. Bannister, and R. Schneider, Histone post-translational modifications—Cause and consequence of genome function, Nat. Rev. Genet. **23**, 563 (2022).
[83] I. B. Dodd and K. Sneppen, Barriers and silencers: A theoretical toolkit for control and containment of nucleosome-based epigenetic states, J. Mol. Biol. **414**, 624 (2011).
[84] D. Menshykau, C. Kraemer, and D. Iber, Branch mode selection during early lung development, PLoS Comput. Biol. **8**, e1002377 (2012).
[85] D. Menshykau and D. Iber, Kidney branching morphogenesis under the control of a ligand-receptor-based turing mechanism, Phys. Biol. **10**, 046003 (2013).
[86] A. G. Larson, D. Elnatan, M. M. Keenen, M. J. Trnka, J. B. Johnston, A. L. Burlingame, D. A. Agard, S. Redding, and G. J. Narlikar, Liquid droplet formation by HP1α suggests a role for phase separation in heterochromatin, Nature (London) **547**, 236 (2017).
[87] A. R. Strom, A. V. Emelyanov, M. Mir, D. V. Fyodorov, X. Darzacq, and G. H. Karpen, Phase separation drives heterochromatin domain formation, Nature (London) **547**, 241 (2017).
[88] S. Sanulli, M. J. Trnka, V. Dharmarajan, R. W. Tibble, B. D. Pascal, A. L. Burlingame, P. R. Griffin, J. D. Gross, and G. J. Narlikar, HP1 reshapes nucleosome core to promote phase separation of heterochromatin, Nature (London) **575**, 390 (2019).
[89] F. Erdel, A. Rademacher, R. Vlijm, J. Tünnermann, L. Frank, R. Weinmann, E. Schweigert, K. Yserentant, J. Hummert, C. Bauer, S. Schumacher, A. A. Alwash, C. Normand, D. P. Herten, J. Engelhardt, and K. Rippe, Mouse heterochromatin adopts digital compaction states without showing hallmarks of HP1-driven liquid-liquid phase separation, Mol. Cell **78**, 236 (2020).